SNPO-C

Astronuclear

WANL-TME-1149
May 1, 1965

(43)

Westinghouse Astronuclear Laboratory

Contribution to the

Twentieth High Temperature Fuel Committee Meeting

May 18, 19, and 20, 1965 (Unclassified)

Prepared by:

A. Boltax and J. M. Tobin

INFORMATION CATEGORY
Confidential-Restricted Data

R. L. Field Jr. 4/28/65
Authorized Classifier Date

(The preliminary information presented in this report should not be published without prior written approval of the Westinghouse Astronuclear Laboratory. The work performed was supported by the Space Nuclear Propulsion Office.

DISCLAIMER

Astronuclear
WANL-TME-1149
May 1, 1965

GENERAL INTRODUCTION

Advances in the high temperature fuel element program for the development of the NERVA nuclear rocket engine will be described. The principal topics will include:

I. EXAMINATION OF NRX-A2 ELEMENTS AFTER HOT TEST

II. NERVA FUEL DEVELOPMENT

III. ANALYSIS OF HYDROGEN CORROSION BEHAVIOR OF NERVA FUEL ELEMENTS.

Astronuclear
WANL-TME-1149
May 1, 1965

I. EXAMINATION OF NRX-A2 ELEMENTS AFTER HOT TEST

(M. Vogel, R. Simmons, D. Jacobs, R. Fiore, and C. Glassmire)

Introduction and Summary

NRX-A2 was the first reactor in the NRX-A series which was tested at rated power conditions. The reactor was tested at Test Cell A, Nevada Test Site on September 24, 1964, at the following conditions of total reactor power and run time.

Power (megawatts)	Time at Power (minutes)
505	1.017
867	0.900
906	0.583
927	0.600
948	2.100
1096	0.650

The fuel elements in the core consisted of hexagonal cross-section, 52-inch long extruded graphite shapes having 19 NbC-coated coolant channels and containing pyrocarbon-coated UC_2 fuel beads.

Following the tests, the reactor was disassembled and components examined at R-MAD. This report summarizes the results of fuel element examination conducted at R-MAD and LASL. A topical report, WANL-TME-1122, has been written which analyzes the effects of the hot test on the fuel elements.

The post-operational examinations of the NRX-A2 fuel elements at R-MAD included gross visual examination, weighing and whole body ionization measurements of all (1626) of the fuel elements in the core. The post-operational studies at LASL included metallographic examinations and flexure strength tests on selected fuel samples from the NRX-A2 core.

From an overall point of view, the NRX-A2 reactor test produced only light surface and channel corrosion in the fuel elements. Heavy surface corrosion resulted on 200 fuel elements as a result of hydrogen leakage inwards from the reactor periphery.

A view of the reactor core during disassembly in Figure 1 shows this corrosion as dark bands at the hot end of the elements. Very light surface corrosion streaks and sooting were produced between 24 to 33 inches from the cold end by interstitial hydrogen attack on the external surfaces of all but 270 of the core fuel elements. The extent of this corrosion is a function of the time at temperature and, thus, is expected to increase during the 20 minute A3 run.

Visual examination established that 58 fuel elements had 1/64 to 1/16 inch diameter pinholes on the surface. The largest number of pinholes were located on eight elements from NbC coating batch C94. Axial distribution of pinholes was concentrated in two regions, 25-30 inches and 45-51 inches from the cold end.

Axial sectioning and metallographic examination revealed the presence of corrosion pockets under the NbC coating as well as general light attack of the graphite binder. This type of behavior was noted between axial station of 20 and 51 inches (from the cold end of the element) which is consistent with the time temperature cycles experienced during the A2 run. Bore corrosion and pinhole formation originating from liner defects is expected to be relatively more significant during the longer A3 run than it was during the A2 run (3-4 minutes).

Metallographic examination of fuel beads indicated essentially no migration of UC_2 from the bead cores due to the reactor test. There was no indication that the maximum fuel element temperature exceeded 2500°C based on the fuel bead examination.

Weight loss analysis of A2 fuel elements indicated an average weight loss of 1.0 ± 0.3 grams for elements with no heavy surface corrosion and with typical bore and end corrosion. The weight loss in peripheral elements with heavy surface corrosion averaged 4.5 grams. Considering weight loss distributions in the core, the total weight loss for NRX-A2 fuel elements was calculated to be 1725 grams.

Length change measurements were made on 35 NRX-A2 elements. The pre-test lengths with orifices in place were estimated to $\pm$ 4 mils. The post-test measurements showed that there was no change in length (3.5 mils average decrease in length)

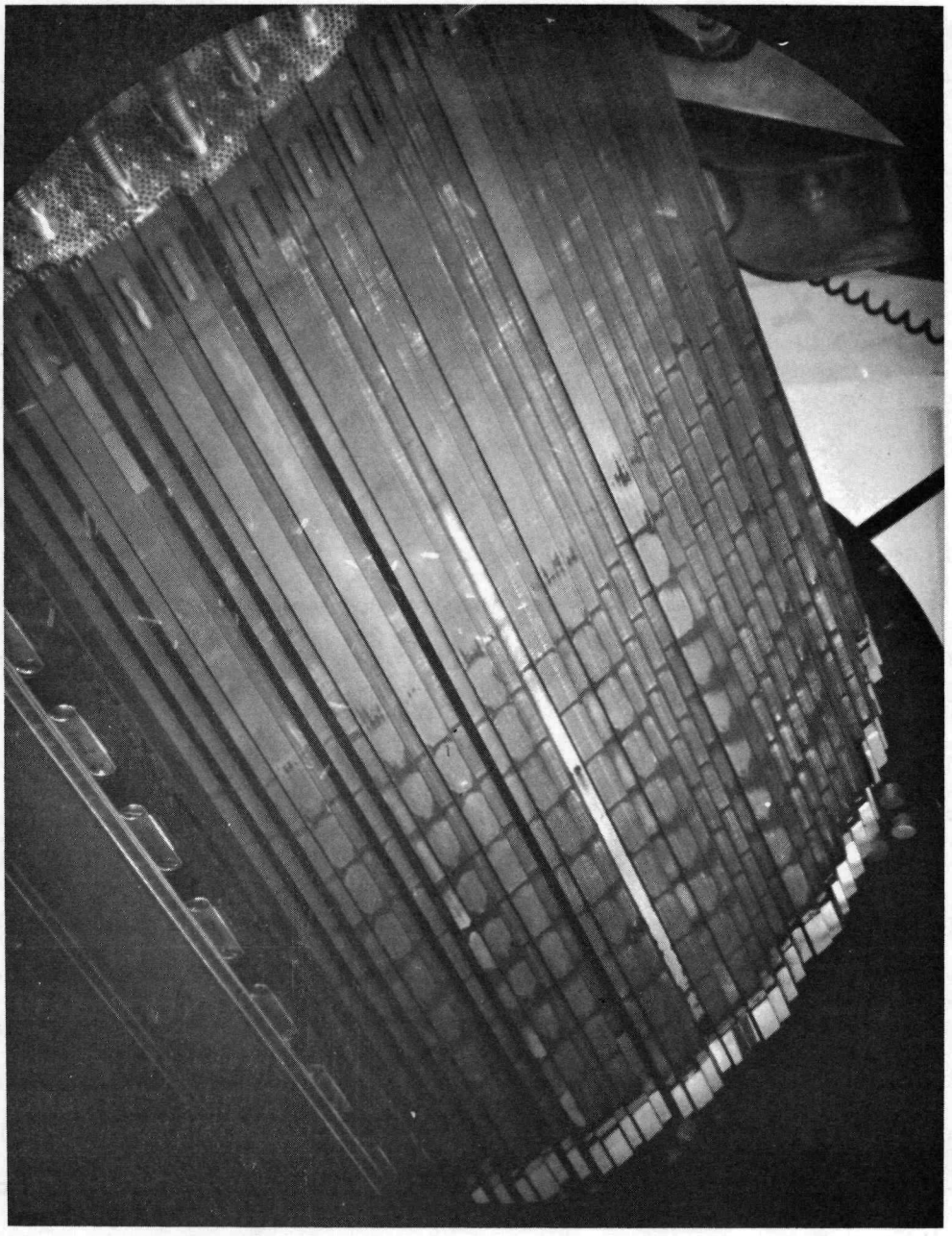

Figure 1 - Tile Pattern Corrosion Bands on Peripheral Fuel Elements of NRX-A2 (Θ = 350° to 75°)

except for four elements. It is reasonable to suspect that the four larger length changes recorded were the result of errors in measurement. The change in the distance across diametrically opposite flat external faces of the elements was measured on 34 NRX-A2 elements at four axial stations. These data indicate essentially no change in across flat dimensions due to the reactor test.

Other significant conclusions which have been derived from the A2 post-operative examinations include the presence of radiation induced property changes in fuel elements at the cold ends. This was evidenced by a 25-40 per cent increase in electrical resistance at the cold end of the elements and 30 per cent increase in flexure strength at the 3-inch station. These effects are consistent with published irradiation data on graphite at the same temperature of irradiation (100°-200°C) and fast-neutron dose (1×10^{18} nvt) as that experienced during the A2 run.

Two significant observations were brought to light by the analysis of the differences between electrical hydrogen corrosion testing and reactor corrosion of fuel elements. One observation suggests that the corrosion rate of fueled graphite may be 2-3 times faster in reactor than determined from the electrical corrosion tests. This observation is tentatively explained by the corrosion-retardation caused by the helium overpressure in use in the electrical tests. The second observation relates to the role of graphite matrix porosity on pinhole formation. It is suggested that further consideration be given to methods for reducing fuel element porosity as one means of minimizing the frequency of pinhole formation. Finally, it is generally concluded that electrical corrosion tests provide a very useful guide for evaluation of fuel elements for reactor testing. It may be expected that significant technical contributions will develop from further careful analyses of the differences in fuel element behavior in electrical vs. reactor tests.

A. Corrosion Effects

Element External Surface Corrosion

Four types of surface corrosion could be distinguished on NRX-A2 fuel elements. These were:

1. Corrosion on external element surfaces on the fuel elements located at the core periphery associated with hydrogen leakage at the pyrotile joints (referred to as tile pattern corrosion).

2. Corrosion at the NbC coated ends.

3. Corrosion associated with hydrogen leakage from thermocouple installations (referred to as T/C associated corrosion).

4. Light corrosion streaks along the length between coolant channel positions from interstitial hydrogen attack.

The heaviest surface effects were produced by tile pattern corrosion, T/C corrosion, and corrosion at the coated ends.

From an overall point of view, the NRX-A2 reactor test produced only light surface and channel corrosion in the fuel elements. Heavy surface corrosion resulted on 200 fuel elements as a result of hydrogen leakage from pyrotile joints and from Station 32 (32 inches from cold end of element) thermocouple installations. The tile related corrosion occurred in ten distinct bands, starting at Station 23 with a separation of 3 inches between bands as shown in Figure 1. Of the heavily surface corroded elements, 41 were observed to have channel NbC liner exposure. These exposures ranged from less than 1 to 5 inches in length and were distributed between Stations 24 and 51. An example of exposure of the NbC liner tubes is given in Figure 2. One element in the core had a single channel exposed for a length of 22 inches due to absence of NbC liner. Five others had channel exposures of less than 1 inch due to corrosion at the shoulder of the coated end. Presence of a partially surface (NbC) coated element in the A2 core demonstrated that this was effective in reducing tile associated corrosion. It is believed that design, material, and operational changes ("fixes") incorporated in NRX-A3 will significantly reduce corrosion from peripheral leakage and thermocouple installations.

Corrosion occurred at the coated end of all but 13 fuel elements in the core. End corrosion typically produced taper and NbC exposure at the hot end and a characteristic corrosion band at the shoulder of the undercut area. A typical hot end of the element is seen in Figures 3 and 4. The least amount of end corrosion occurred on elements which had

Figure 2 - Liner Exposure Produced by Tile Pattern Corrosion at Stations 49-51 on the D Flat of Element 32-11765, Core Position 1J7J

CONFIDENTIAL
RESTRICTED DATA
Atomic Energy Act - 1954

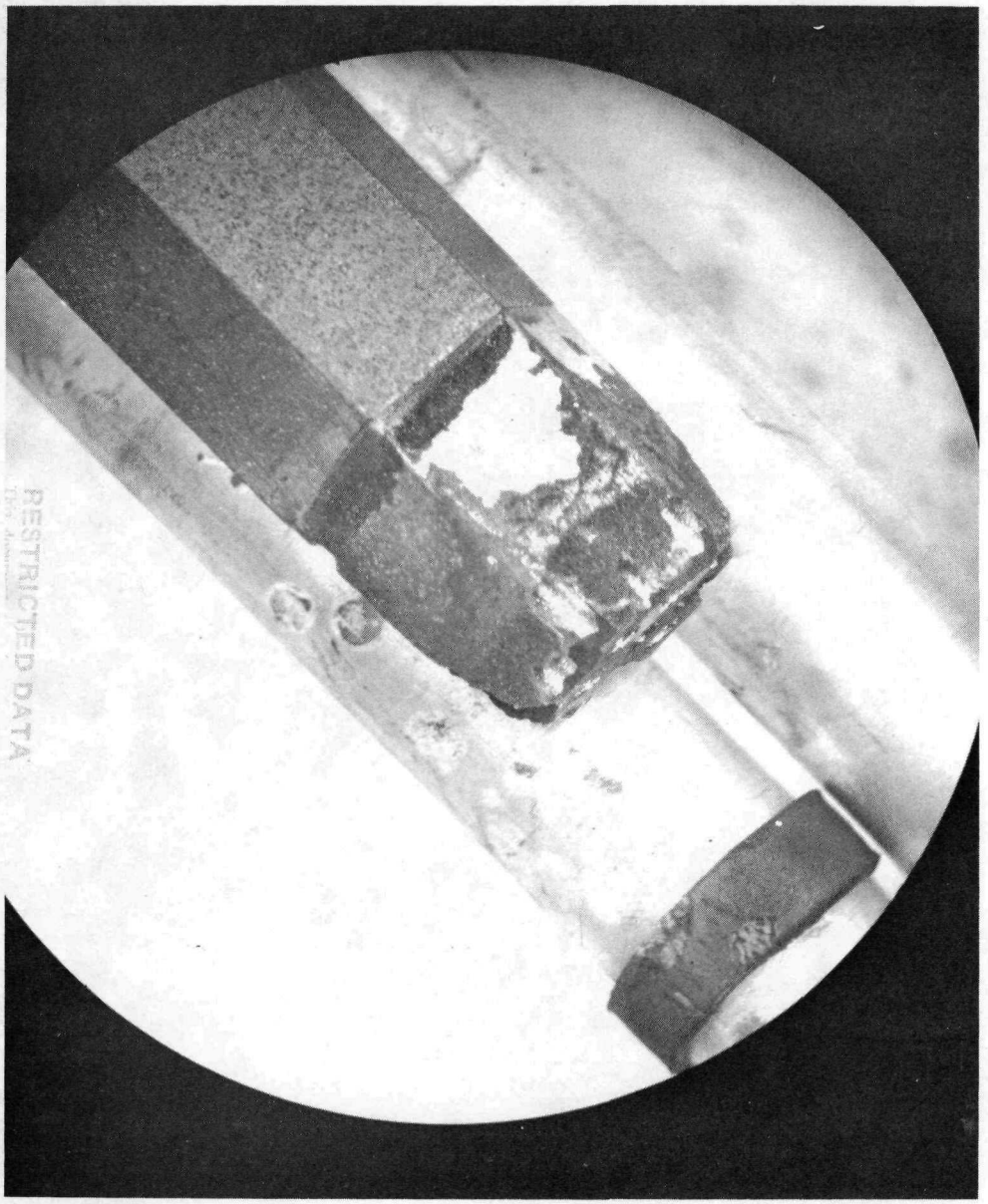

Figure 3 - Typical Corrosion Taper of Coated End Flats with Corrosion Band at the Shoulder on Element 99-07086, Core Position 2A1G

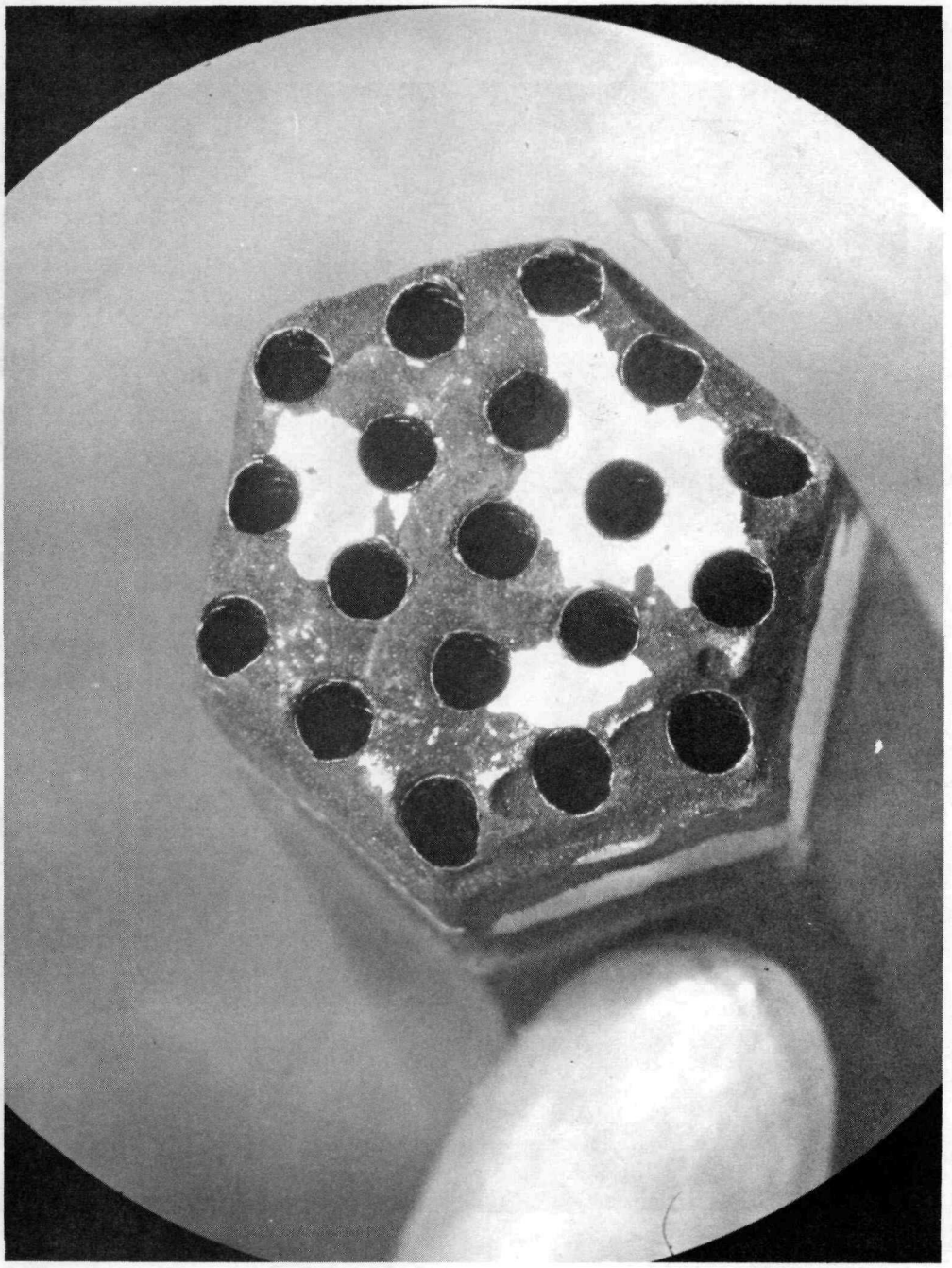

Figure 4 - Typical Corrosion on Exit Face of Element 99-09313, Core Position 4A1D. The coated area remaining (CAR) is about 40% and the bearing area remaining (BAR) about 70%.

been recoated at Oak Ridge, Y-12. The addition of an unfueled wafer tip to the coated end of NRX-A3 fuel elements should significantly reduce the type of end corrosion observed in NRX-A2 elements.

1. Tile Pattern Corrosion - The peripheral elements in NRX-A2 displayed surface corrosion patterns on exterior flats which corresponded to the hydrogen leakage at the pyrotile joints. This corrosion occurred in 10 distinct transverse bands extending from Station 23 to 51; the bands having an axial separation of approximately 3 inches. Typical tile pattern corrosion effects are shown in Figures 1 and 2.

Of the 156 peripheral elements in the NRX-A2 core, 153 had tile pattern corrosion on exterior flats. Two peripheral elements (1J6K and 5J9U) had only light corrosion streaks with no evidence of tile effects. It is presumed that the filler block joints associated with these latter two elements were tight enough to restrict hydrogen leakage.

One peripheral element (6J8D) had considerable NbC coating on its exterior flats as a result of "flash back" during bore coating. This coating effectively inhibited tile pattern corrosion at all Stations except 26, 33, and 51. Samples from the 30, 37, and 48-inch stations were examined metallographically so that the relationship between coating thickness and corrosion could be ascertained.

The depth of tile pattern corrosion was determined on twelve elements. The measurements were made along the centerline of each corroded flat and did not include measurements in those regions of channel exposure. The maximum depth of corrosion occurred at the 39-inch station. This distribution was probably the result of non-uniform radial hydrogen leakage, since the axial temperature distribution in the fuel elements and corrosion data predict an exponentially increasing corrosion with increasing axial station.

Tile pattern corrosion produced liner exposures at 31 positions on 17 peripheral elements. The axial range of exposure was from Stations 24 to 51; of the total number of exposures, 45 per cent occurred at Stations 35 to 45 and 35 per cent occurred at Stations 49 to 51. The length of channel exposure due to this effect varied from less than 1-inch to 3 inches. Figure 2 shows the typical appearance of liner exposure associated with tile pattern corrosion.

2. Corrosion at the NbC Coated Ends - Most of the fuel elements in NRX-A2 exhibited corrosion at their coated ends. This corrosion occurred at the exit face, on the flats and as a corrosion band at the shoulder area. In general, the corrosion on the exit face and end flats caused a tapering of the hot end and exposure of the NbC coating. The typical effect is shown in Figures 3 and 4. Seventeen fuel elements showed no corrosion on the exit face. Thirteen exhibited no corrosion on the end flats. Six of the thirteen had been recoated at Oak Ridge, Y-12.

In order to relate the observed coated end corrosion behavior to the pre-test hydrogen corrosion rating of the elements, an analysis was performed on 1,525 fuel elements from the core. The analysis was performed on the basis of three categories of exit face condition.

(1) Those elements with a bearing area remaining (BAR) of more than 70 per cent (better than typical),

(2) Those with a BAR of about 70 per cent (typical), and

(3) Those with a BAR of less than 70 per cent (worse than typical).

A survey of the end corrosion in Sectors 1 and 3 of the core revealed that end corrosion effects did not vary appreciably from the center of the core to the periphery.

3. Thermocouple Associated Corrosion - Several fuel elements in the vicinity of thermocouple installations exhibited heavy surface corrosion patterns. These were attributed to the leakage of hydrogen from thermocouple slots in the unfueled elements. The corrosion associated with the 20 and 45-inch station thermocouples was generally light and involved only those elements immediately adjacent to the thermocouple slot. Generally, the corrosion on these fuel elements started at about the 31-inch station and extended varying distances to the hot end.

4. Streaking - Dark streaks were observed on the flats on all but 270 of the NRX-A2 fuel elements occurring generally at about mid-length positions. The streaks occurred on one or more flats of each element and were typically displayed as two parallel dark lines located on the flats at positions between the underlying coolant channels as

shown in Figure 5. The streaks were not always continuous, some being interrupted in the axial direction. Detailed visual examinations of the phenomena indicated that no significant depth of corrosion was involved. These data indicate that the major occurrence was at Stations 24 to 33 with very little change in axial location as a function of core radius. Although the exact mechanism is not known, the streaks observed are believed to be the result of light corrosion by interstitial leakage of hydrogen at the upstream positions of the streaks with subsequent soot deposition on downstream portions of the fuel element flats.

Samples cut from fuel elements which exhibited streaking were examined metallographically. No unusual microstructural changes were observed at the element surfaces affected.

Coolant Channel (Bore) Corrosion

1. NbC Liner Undercutting - Twenty-one fuel samples were examined metallographically specifically for liner-substrate condition. Generally, undercutting corrosion of NbC liners was observed from Stations 20 to 51. The maximum depth of undercutting occurred at approximately the 30-inch station.

The NbC bore coatings on the NRX-A2 fuel elements were applied at about 1900°C (2173°K). The coefficients of thermal expansion of NbC and the graphite are quite dissimilar; that of graphite being less than that of NbC. Consequently, the liner was permeated with numerous small cracks when held at temperatures less than 1900°C. As a result, the graphite beneath these cracks can be exposed to hydrogen during reactor tests. If the temperature is sufficiently high for corrosion to occur, the graphite substrate will be attacked leaving a void (undercutting) beneath the NbC liner.

The rate of undercutting (R_U) can be described by the relationship

$$R_U = \beta (2173 - T) \exp(-Q/RT) \quad (1)$$

where

β = constant

T = temperature, (°K)

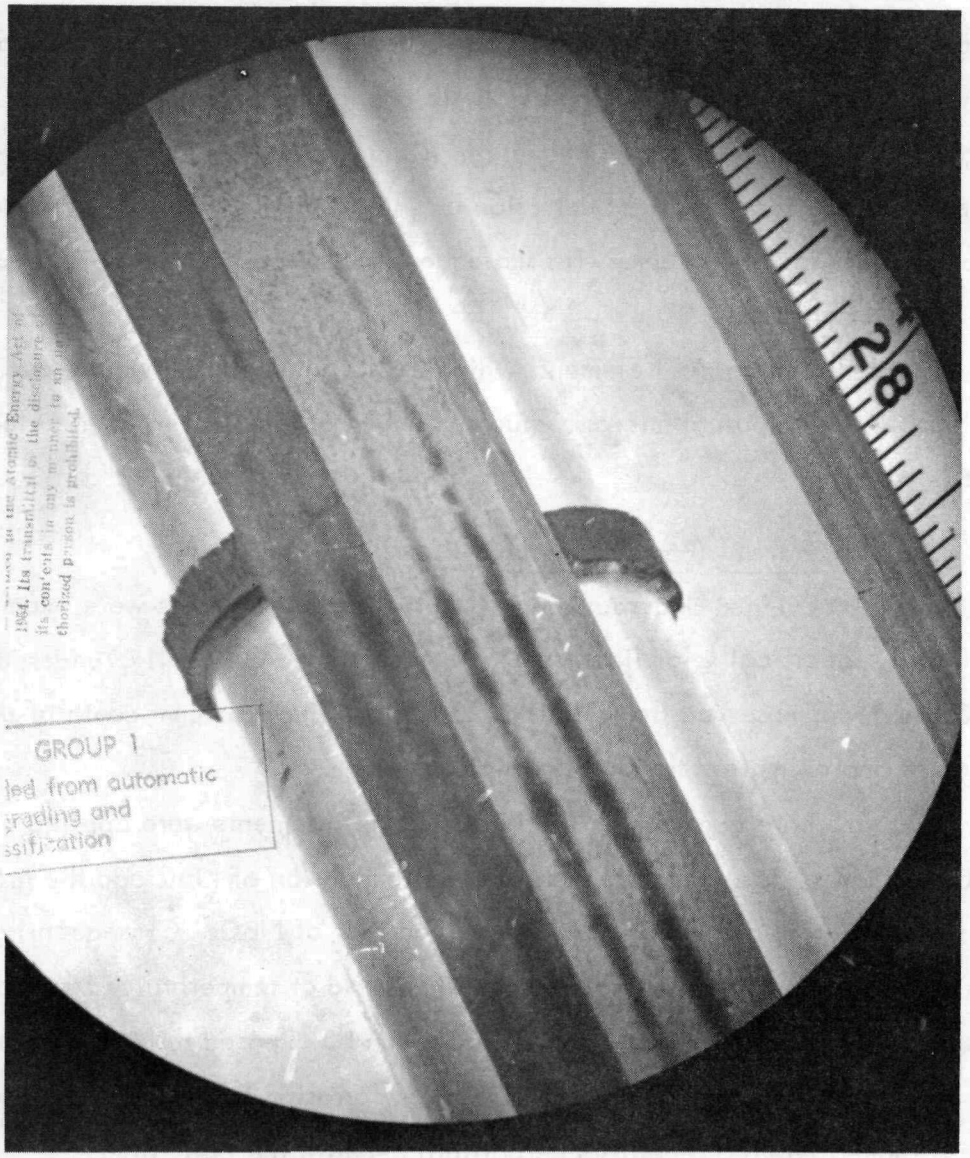

Figure 5 - Streaking on the C and D Flats of Element 89-11877
Core Position 1J5G, at Stations 27-29

Q = activation energy

R = gas constant.

Data collected from the hydrogen corrosion testing performed at WANL indicate that Q = 30,000 calories. Using this value for Q, Equation 1 predicts a maximum rate of undercutting at 1630°C.

The relative depth of undercutting at various axial stations in NRX-A2 was calculated using the expression

$$D_u = \sum_{i=1}^{6} t_i(2173 - T_i) \exp(-30,000/RT_i) \quad (2)$$

where, t_i = duration of the i^{th} power hold at temperature T_i(°K).

The data obtained from the metallographic observations are plotted in Figure 6. These data were obtained by measuring the depth of undercutting immediately below cracks in the NbC liner. Measurements of this kind are somewhat inaccurate but they suffice to show general trends. The agreement between the calculated and measured values appears good.

2. Pinholes and Corrosion Pockets - Fifty-eight NRX-A2 fuel elements developed pinholes. Forty-two of these elements had 1A hydrogen corrosion channel ratings and sixteen had 1C channel rating. Considering all of the fuel elements in the core, these data show that 3.1 per cent of the 1C rated and 3.8 per cent of the 1A rated elements in NRX-A2 showed pinholing. The results indicate that the A and C rated elements behaved about the same with respect to pinholing. Of the fifty-eight elements, thirty had only one pinhole. A relationship between coating batch and pinholing was found. The largest fraction of pinholed elements were from coating batch C94. The process history of coating batch C94 was essentially the same as that of the other coating batches represented in the core.

The axial distribution of pinholes in NRX-A2 showed two maxima occurred at the 25-30 and at the 45-52 inch stations. The explanation for this phenomenon will be discussed in detail later. The appearance of pinholes as observed on the fuel element

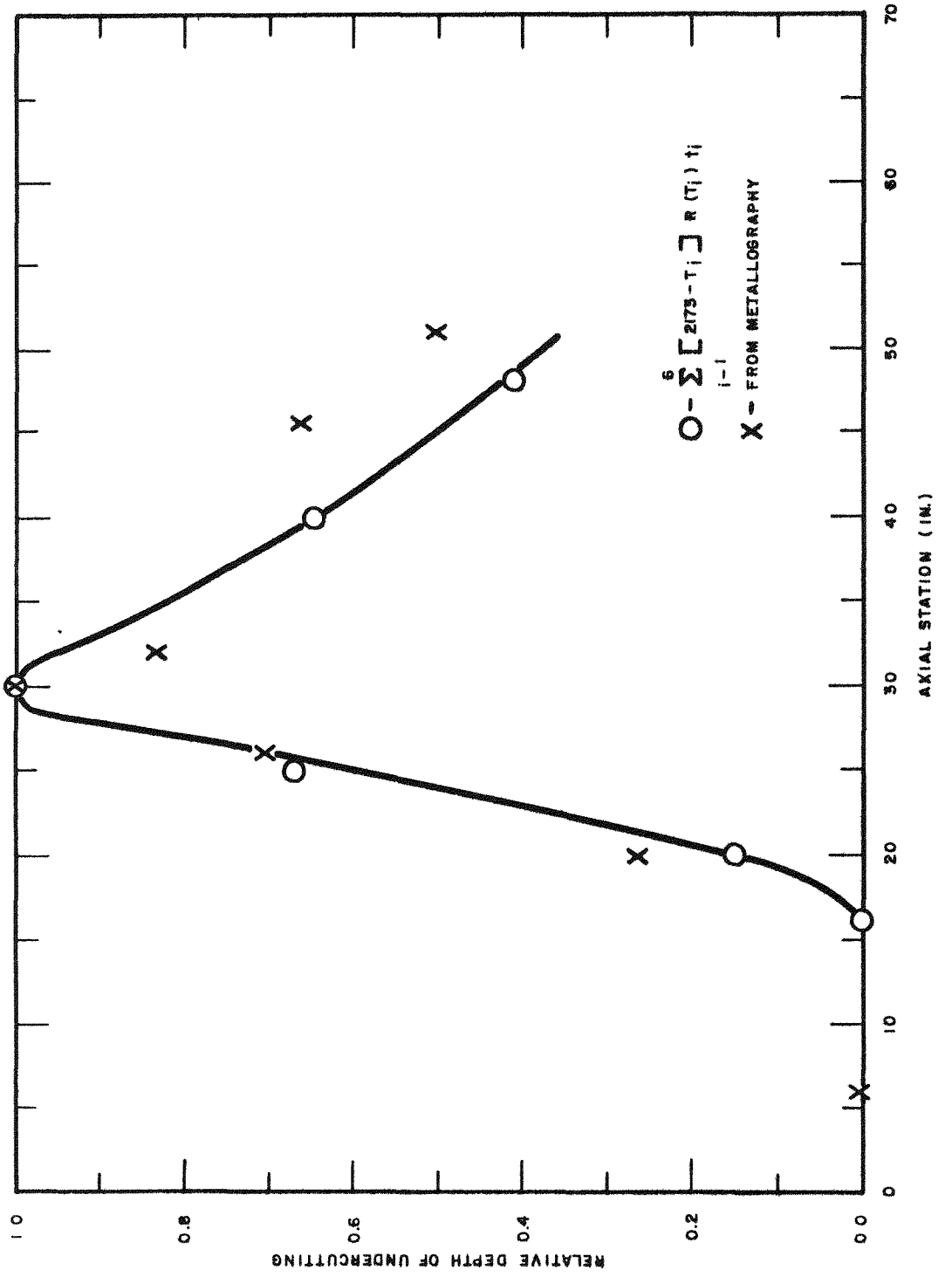

Figure 6 - Relative Distribution of Liner Undercutting-Data Normalized to 1.0 at 30-inch Station

surface is shown in Figure 7. Figure 8 is a photo-micrograph of a typical pinhole.

Thirty fuel elements from NRX-A2 were sectioned axially through Channels 8, 9, 10, 11, and 12 and given detailed visual examinations. Of these, four elements exhibited corrosion pockets.

Pinholes and corrosion pockets occur when a segment of the NbC liner is defected. This is illustrated by Figure 9. Generally, these defective segments are larger than the normal differential contraction cracks and consequently, corrosion in these local regions will proceed more rapidly than in the case of liner undercutting. Depending upon orientation and the extent of attack, a corrosion pocket may either reach the surface (forming pinholes) or it may reach neighboring coolant channels. The latter phenomenon was not observed in NRX-A2. However, it was obvious that inter-channel communication would have occurred had the duration of the test been greater.

The greater frequency of pinhole occurrences in the axial regions 25-30 inches and 45-51 inches is not clearly understood. Calculation of the extent of corrosion of uncoated fueled graphite indicates that pinholes would be expected at axial stations beyond 34 inches. The equation used for this calculation is given below:

$$D = \sum_{i=1}^{6} 7 \times 10^{5} t_i \exp(-30,000/RT) \qquad (3)$$

where D is corrosion depth in mils, and t_i and T_i are the time in hours and the temperature in ^{o}K of the i^{th} reactor power hold period of time.

The calculations indicate the corrosion depths of 6-15 mils would be expected at the 25-30 inch stations. Consequently, corrosion of fueled graphite through coating defects would not account for pinholes observed at these stations. Evidence of corrosion through graphite pores was seen indicating that graphite matrix porosity can play a major role in pinhole formation.

Spots of surface corrosion (referred to as dimples) were noted on several fuel elements in NRX-A2. These spots were found to be associated with pinholes on adjacent fuel elements and are believed to be the result of hydrogen gas exiting from the pinholes.

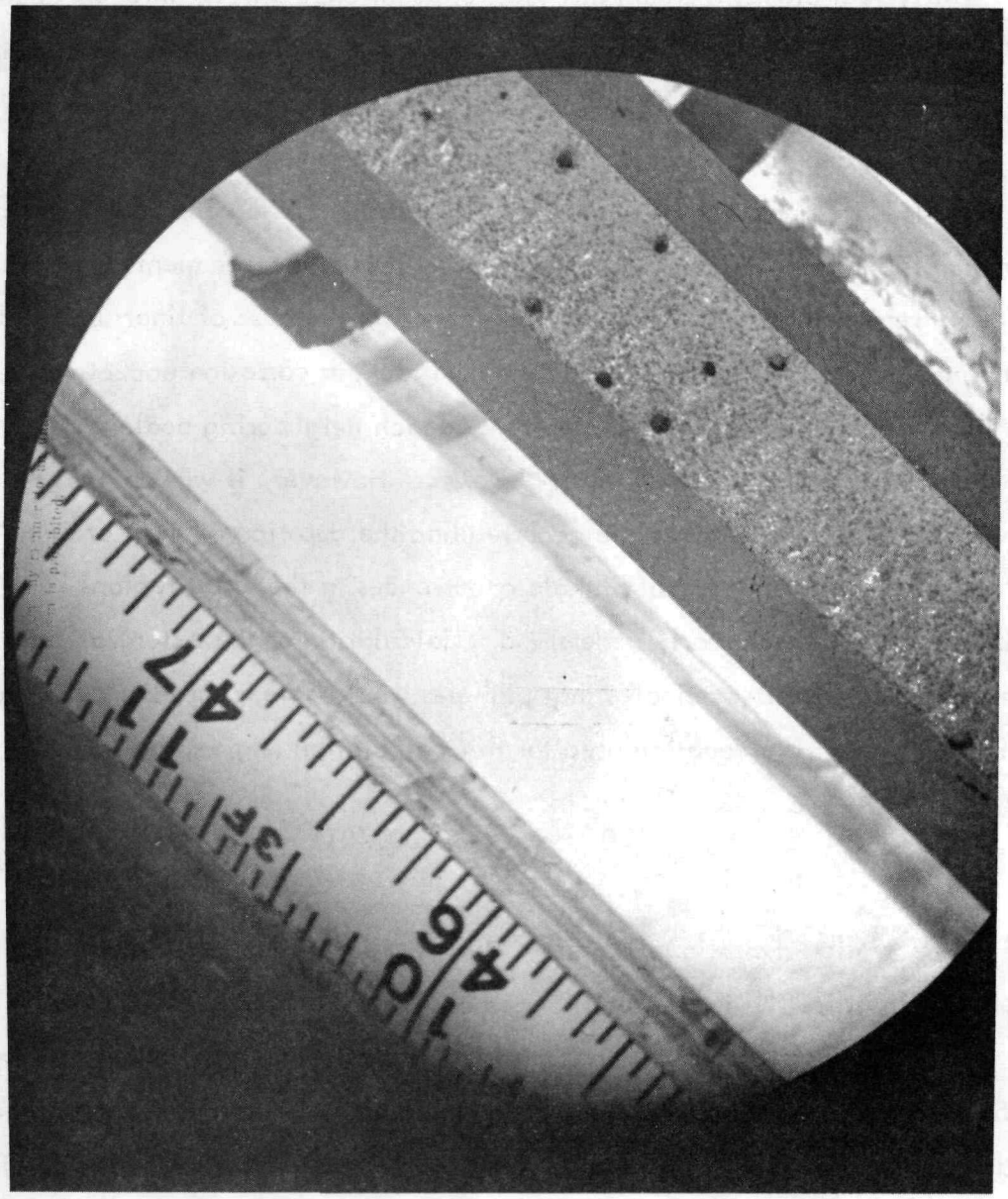

Figure 7 - Pinholes on the A Flat of Element 99-07089, Core Position 4E4E, at Stations 45 to 48

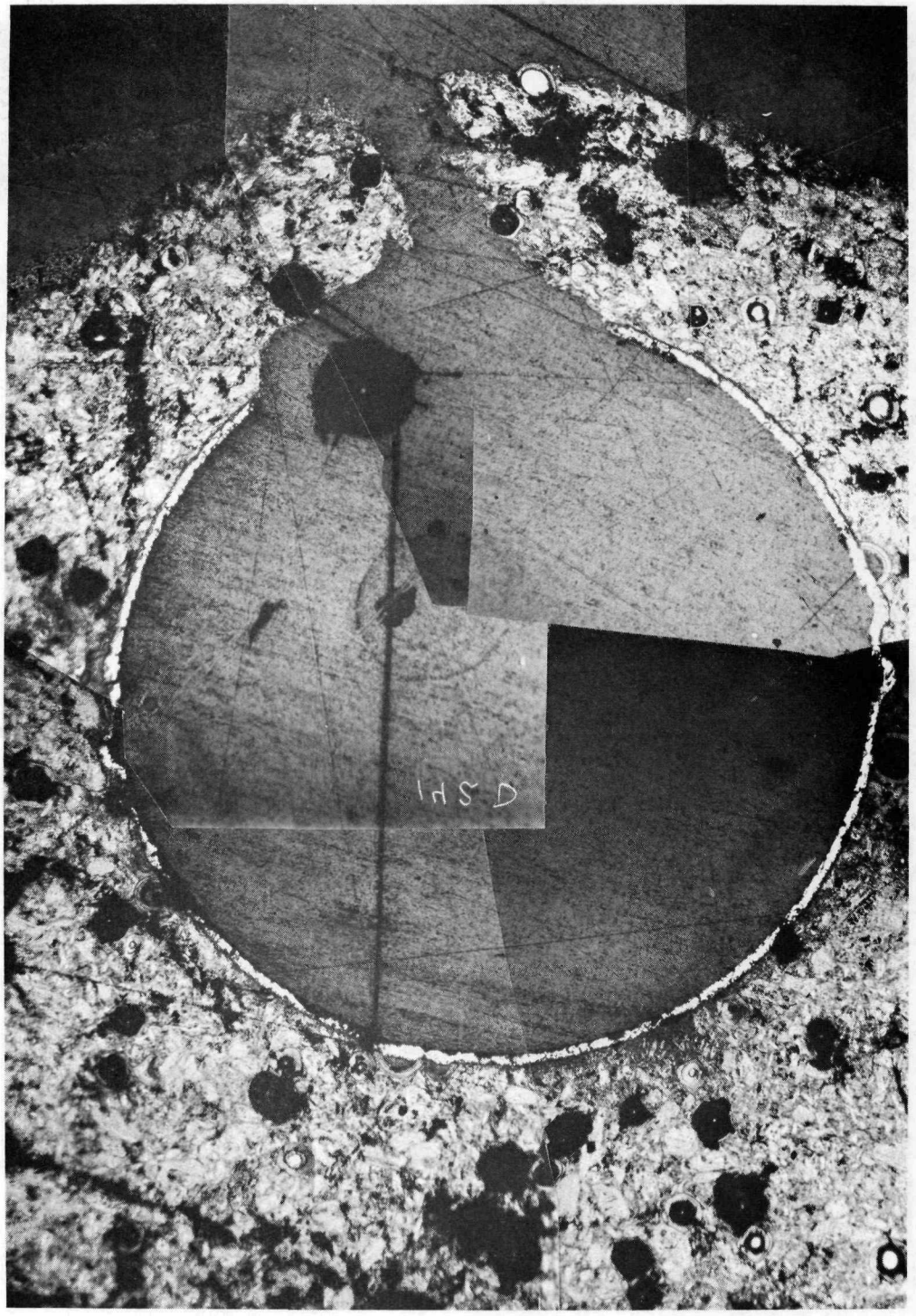

Figure 8 - Photomicrograph of a Pinhole in Element 3G1D, Channel No. 8, Station 20

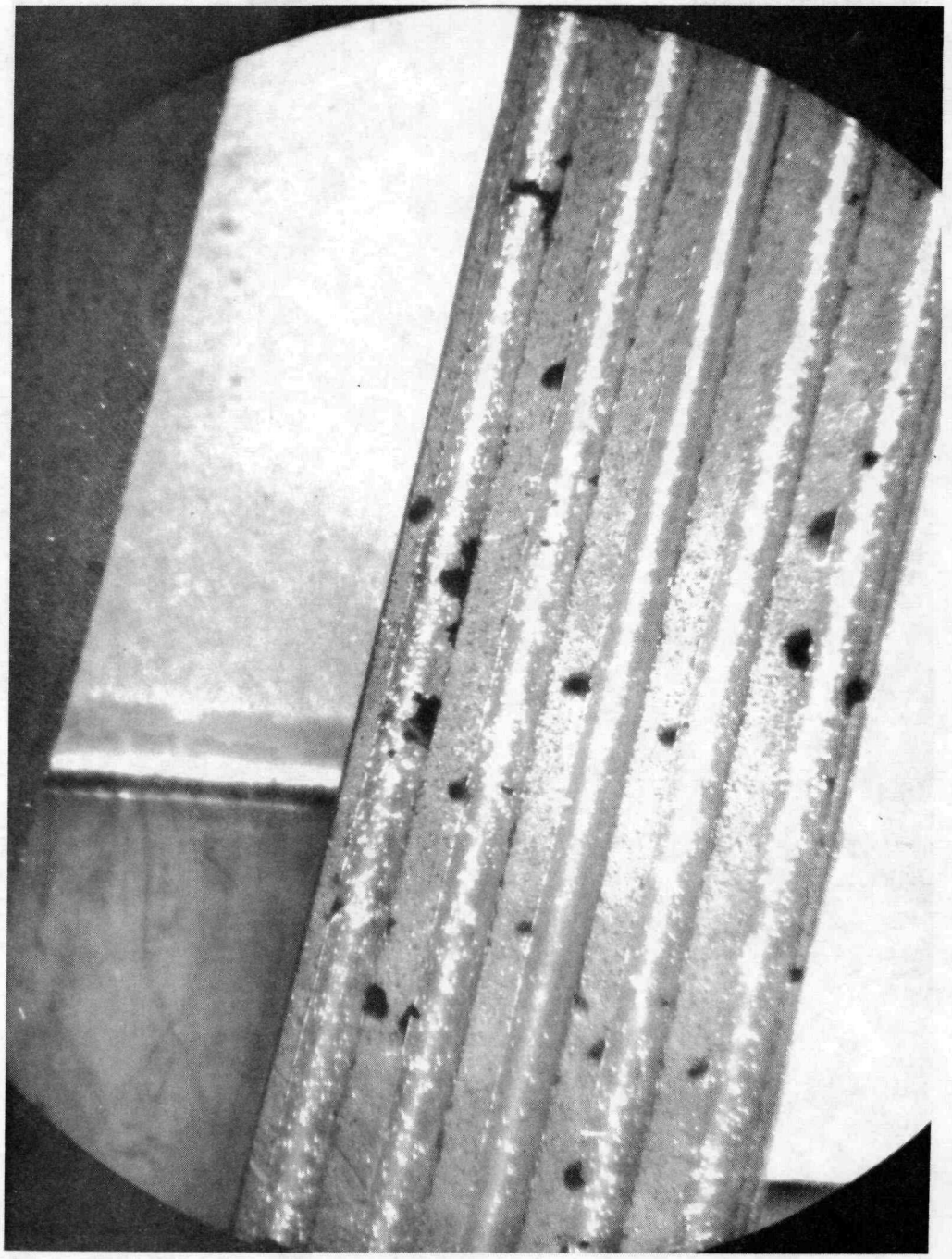

Figure 9 - View of Channels 8, 9, 10, 11, and 12 at Stations 47-50 on Element 99-07089, Core Position 4E4E, Showing Corrosion Pockets and Pinhole Formation

Corrosion of a coolant channel in the absence of an NbC liner was observed to be extensive as shown in Figure 10.

B. Flexure Strength

Flexure strengths were determined at LASL on 36 five-inch long fuel samples sectioned from nine NRX-A2 fuel elements. Averaged post-test strengths as a function of axial station are plotted in Figure 11 and are compared with the pre-test data. While standard deviations are somewhat large, these data indicate an increased strength in the cold end samples which decreases toward the hot end where it approximates the pre-test level. Similar effects at the cold end have been noted in KIWI tested fuel elements. The increased strength at the cold end of NRX-A2 fuel elements is believed to be due primarily to radiation effects. The dotted line in Figure 11 represents the general change observed in the KIWI elements normalized to the pre-test strengths for NRX-A2 elements. The results show comparable trends at the cold end although the inflection at Station 26 observed for KIWI elements was not seen in NRX-A2 elements.

C. Incremental Electrical Resistance Changes

The pre- and post-test electrical resistance was measured at 1-inch increments from Station2 to 50 on the "a" flat of 74 fuel elements from NRX-A2. Tile pattern corrosion effects produced regular resistance peaks corresponding to the occurrence of the corrosion bands. The effect of pinholing on electrical resistance was not generally observed on the NRX-A2 elements except in those cases where several pinholes occurred in a limited axial region.

In general, typical profiles indicate an increase in resistance at the cold end and a general peaking in ΔR (difference between pre- and post-test data) in this region, which is believed to be the result of radiation effects and not effects related to bore corrosion and liner defects. There was a 25-40 per cent increase in electrical resistance noted at the cold end of the element. This is consistent with published irradiation data on graphite irradiated at temperatures of 100°-200°C to total fast neutron doses of 1×10^{18} nvt. A survey of the axial position of the maximum ΔR on all of the 74 fuel

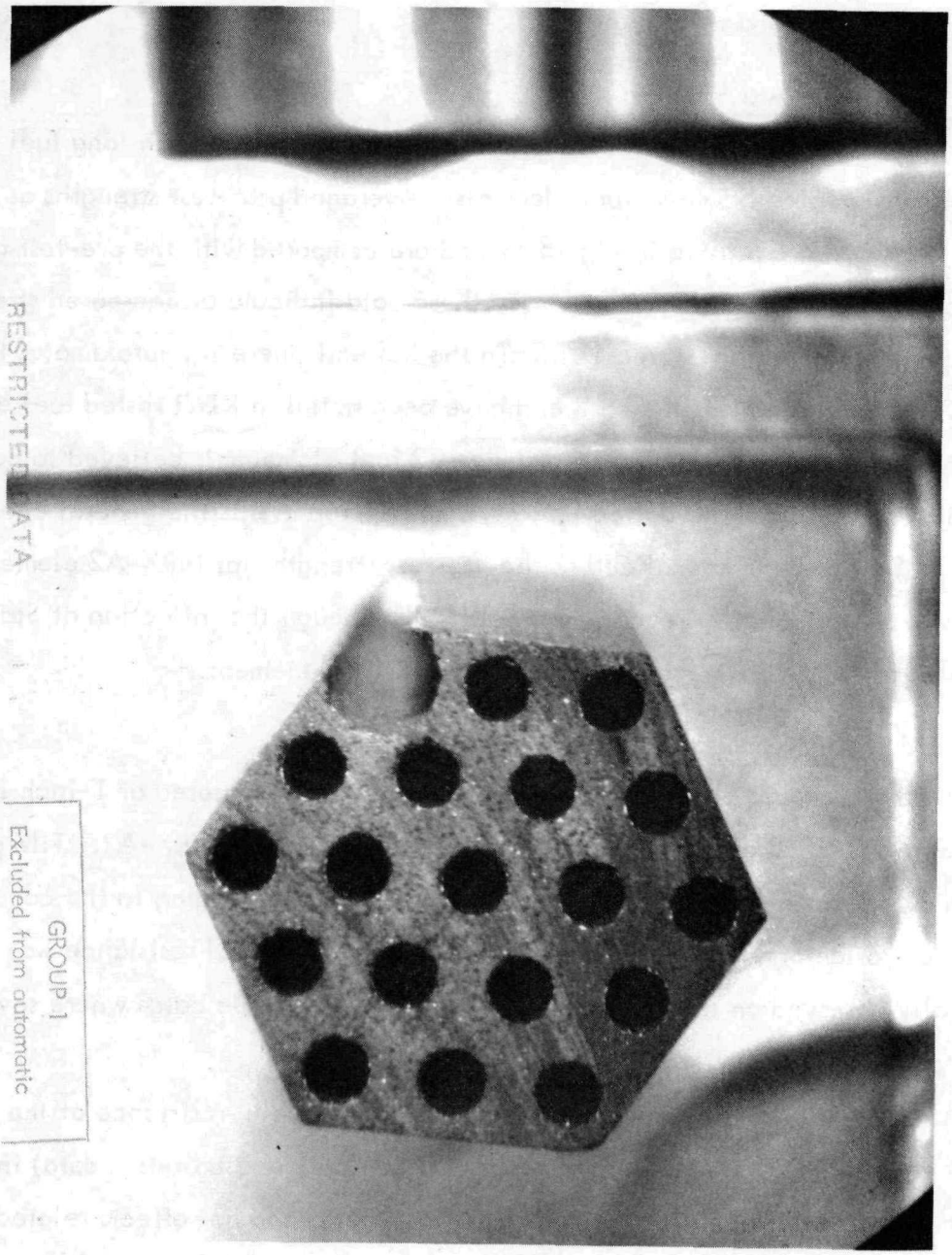

Figure 10 - View of Corroded Channel 3 at Station 47 on Element 5F4F

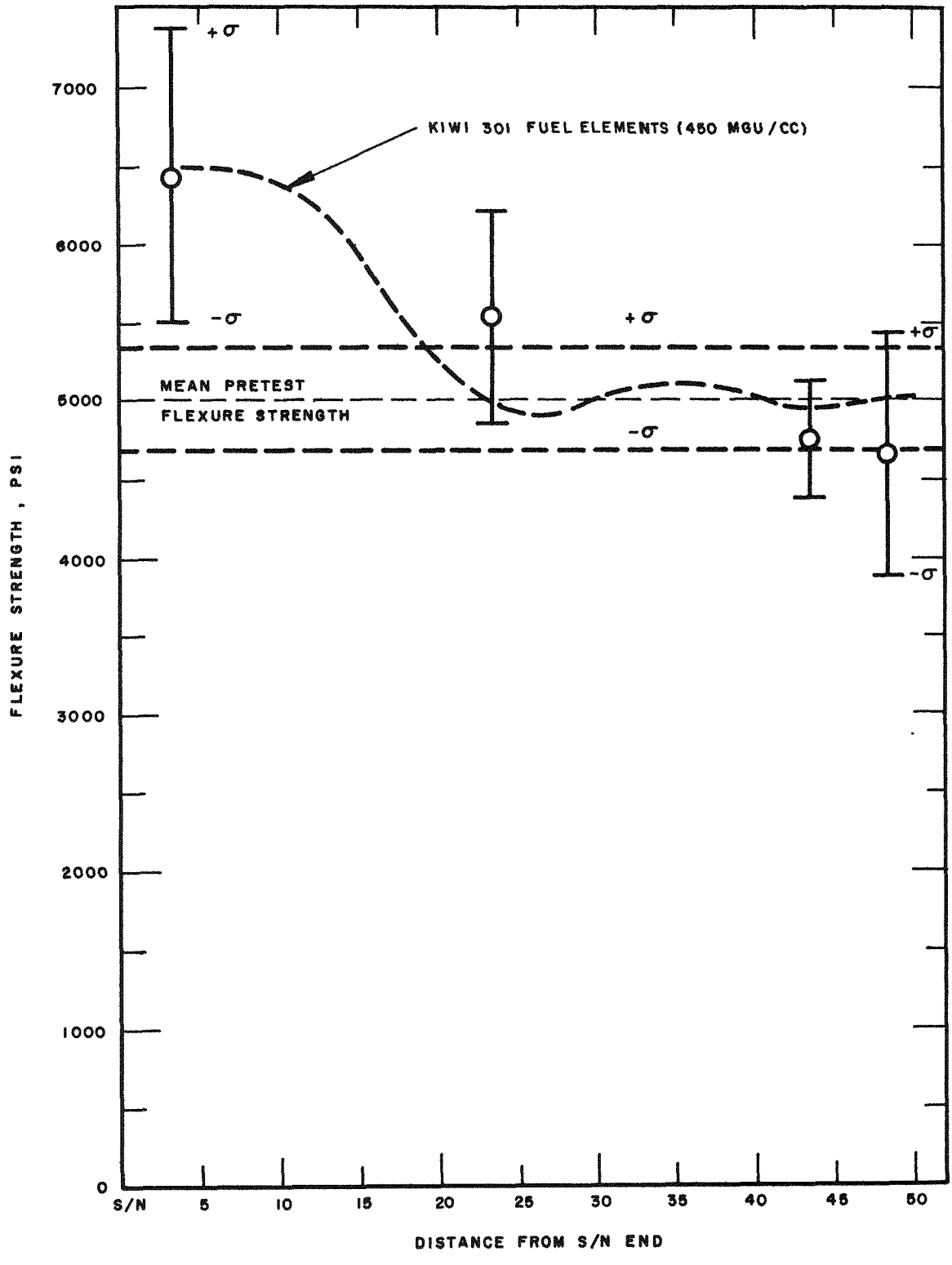

Figure 11 - Flexure Strength After Reactor Test
(NRX-A2 Fuel Elements Compared to KIWI-301 Fuel Elements)

elements indicates that the peaking occurred predominately at about Station 20. There was no indication of a shift in this peak as a function of core radius. The position of the maximum ΔR occurred about 5 inches upstream of the axial location of maximum pinhole occurrence and 10 inches upstream of the region of maximum undercutting. It is possible that the radiation effect was of sufficient magnitude to overshadow the effect of bore corrosion and liner defects. Significantly, while bore corrosion effects were noted, this corrosion was generally light and may not have had a significant influence on the resistance as measured. It should be noted that the ΔR peaks were generally very broad around Station 20 and nominal resistance changes due to bore corrosion could have been masked. Planned electrical resistance measurements on NRX-A3 fuel elements will be conducted using 1/2-inch measurement increments to obtain higher sensitivity to bore corrosion effects.

The post-test resistance profiles indicated that very little graphitization or fuel migration had occurred in the elements since the resistance in general did not decrease below pre-test values at Stations 35 to 50.

Figure 12 gives the ΔR curves for a typical IC reactor-tested element which had insignificant surface corrosion and for an IC element tested in the electrical corrosion test. The major difference in the profiles is a shift of the cold-end ΔR peak in the reactor tested element toward upstream stations by about 3-4 inches. The profiles show similar changes at the hot end. The relative agreement between the two profiles indicates that the NRX-A2 element probably saw maximum temperatures comparable with those of an IC test (2120°C surface).

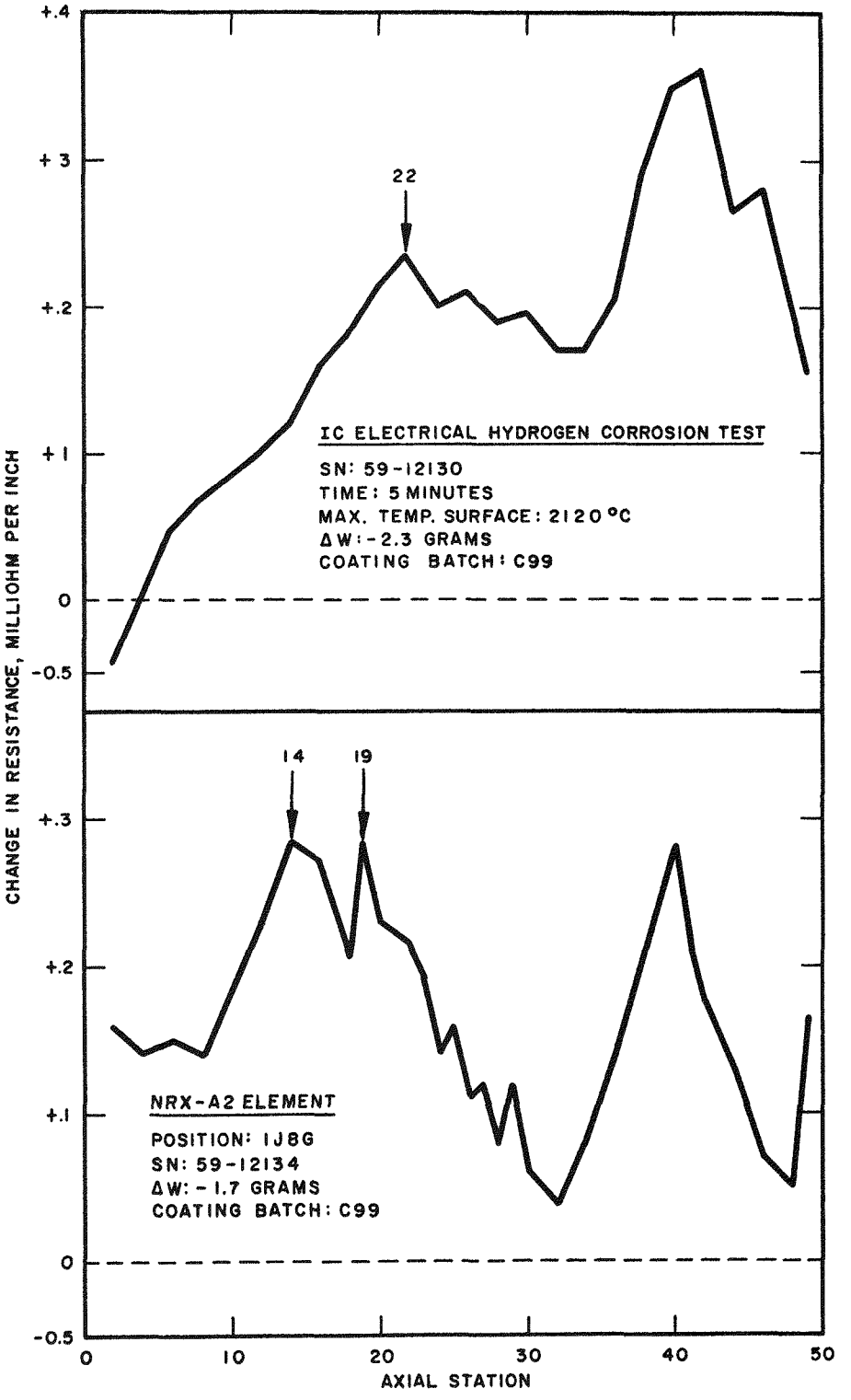

Figure 12 - Comparison of Changes in Electrical Resistance Profiles for an NRX-A2 Fuel Element and a H_2-Tested Production Fuel Element from the Same Coating Batch

II. NERVA FUEL DEVELOPMENT

(M. Tobin, L. Adelsberg, W. Brizes, L. Cadoff, and R. Patterson)

Summary

A major improvement in the bonding of graphite fuel element parts has been found in the development of the liquid-phase zirconium (LPZ) brazing process. The coating of graphite fuel element surfaces with ZrC by the LPZ process has also been developed and shows promise for a hydrogen corrosion protective coating on graphite. Decarburization experiments with NbC in hydrogen have indicated an advantage in hot hydrogen corrosion protection of graphite may be obtained by the intentional addition of a fraction of a per cent of methane to the hydrogen. Carbon diffusion experiments in TaC indicate that a coating of TaC may be superior to NbC as a carbon diffusion barrier at high temperatures (above 2000°C).

A. Brazing and Coating of Graphite - Fuel Element Brazing

The present NRX reactor designs require the cementing of an unfueled tip to the end of each fuel element. Carbonaceous cements used thus far in this work have been able to yield joints with approximately one half the strength of the base element. While this level of strength has been adequate in current core designs, it would be advantageous to significantly increase the strength of the joints and allow more flexibility in core design. Recent encouraging results have been obtained using Zr metal as a braze which is subsequently carburized to ZrC. Commercial ATJ graphite was brazed under pressure using Zr metal with a resultant joint of equal strength to the base material. Subsequently, several experiments were performed using NERVA fueled material and unfueled graphite with similar results. A more intensive program is now underway in which several variables such as pressure during brazing and thermal treatments are being investigated to determine the optimum brazing conditions.

The current brazing process is a four step process consisting of

(1) The placement of a zirconium metal foil (2 mil thickness) between the two graphite members,

(2) The application of a load of approximately 1000 psi,

(3) The rapid heating (less than 30 seconds) of the joint to 2100°C, and

(4) The joint is then held at 2100°C or higher for thirty minutes to insure complete formation of ZrC.

The most important step in the process is the melting of the zirconium metal before it is completely carburized to ZrC. The process mechanism is the wetting of the substrate by the liquid metal; ZrC is refractory (ZrC + C eutectic at 2890°C) and thus, cannot wet the graphite at temperatures below 2890°C.

Once the Zr - C bond has been formed, it is advantageous to heat the joint to higher temperatures because of the temperature dependence of the growth rate of ZrC, and thus minimize the process time. An activation energy of 95,000 cal/mole has been measured for the growth rate of ZrC formed by zirconium carbon reaction.

Pure zirconium metal is used for this application since the resulting ZrC bond is very refractory. The ZrC + C eutectic temperature has been determined to be 2890°C. A lower melting braze alloy is also being developed for use in the lower temperature regions of the core. The eutectic 70 Zr-30 Cu alloy has excellent wettability and forms good bonds at 1100° to 1200°C. The melting point of the eutectic is 995°C. The rate of carburization is slow at the braze temperature and the alloy bond remains strong, ductile, and metallic.

ZrC Coating of External Fuel Element Surfaces

Another application of the wettability of liquid-phase-zirconium coatings is in the formation of a thin, strongly adherent ZrC coating for use as an external protective coating on fuel elements. This process can afford external protection to the elements and may have potential as a technique to seal peripheral leaks in cemented joints fabricated by present carbon cement processes.

The procedure for the coating process is to apply the metal as 0.010 inch diameter wires to the surfaces to be coated and then rapidly raise the temperature to just above the melting temperature of the metal. The molten metal will flow over the surface and

subsequently carburize to ZrC. The temperature can be raised after melting occurs if more rapid carburization is desired. The temperatures and rates of heating vary with different applications and work directed toward establishing these parameters is proceeding.

B. Decarburization of NbC by Hydrogen

Hydrogen flowing over the NbC bore coats in the NERVA fuel element results in a lowering of the C/Nb ratio to approximately 0.75 (i.e., NbC) at the exit end. Undercutting of the coating occurs which apparently results from carbon diffusion through the relatively crack-free coating. The driving force for the diffusion is controlled by the carbon concentration gradient across the NbC coating resulting from decarburization by the hydrogen. Experimental evidence has been obtained which indicates a strong reduction in the rate of decarburization of NbC by hydrogen containing small concentrations of carbon. In flowing carbon-free hydrogen, a fully carburized NbC 10 mil wire filament was decarburized to Nb metal at $2300^{\circ}C \pm 100^{\circ}C$. The observed C/Nb ratio of 0.75 in the NbC bore coats has been calculated to be the equilibrium stoichiometric ratio in contact with hydrogen containing only 4×10^{-5} mole per cent carbon (as hydrocarbon such as CH_4 or C_2H_2). This agrees well with observed carbon losses in corrosion tests. If the carbon content were increased to 2×10^{-4} mole per cent, the equilibrium stoichiometric ratio at $2400^{\circ}C$ would be 0.95.

This suggestion of intentional carbon doping of the hydrogen coolant reactivates an old idea in the graphite matrix nuclear rocket technology which involved the addition of CH_4 to reduce the carbon loss from the graphite. The amount of carbon needed to reduce decarburization of NbC is small. At a core flow rate of 72 pounds hydrogen per second, a carbon injection of 60 to 180 pounds per hour of operation is required. This could be added as CH_4, but a pre-placement of a sacrificial coating of pyrocarbon in the bores may accomplish the carbon doping without the tankage and plumbing required by the CH_4. A PyC coating of 1 mil thickness deposited upon the current NbC bore coat over the axial length from 10 to 40 inches would add approximately 6 grams of carbon per

element. Corrosion of this carbon in the lower temperature regions would presumably protect the hot exit end of the element.

C. Carbon Diffusion in ZrC, NbC and TaC - Zirconium-Carbon System

The reaction between liquid zirconium and carbon at temperatures between 2000° and 3000°C has been investigated. The reaction products were found to be carbon saturated zirconium metal and solid ZrC. The latter formed a layer between the two reactants as shown in the metallograph in Figure 13. At all temperatures of this study, the ZrC layer grew proportionally to the square root of time. The thickness of the ZrC layer as a function of the square root of time is shown in Figure 14. The parabolic rate constant, K_p, for ZrC growth is shown as a function of reciprocal temperature (1/T) in Figure 15 and was found to be 14.3 exp (-95,000/RT) cm^2/sec. At 2725°C an anomaly appears in the K_p vs. inverse temperature curve. The reason for the anomaly has not been conclusively established yet.

The Zr(liq)/(Zr(liq) + ZrC) phase boundary over the temperature range 2000° to 2800°C was determined. The results are shown in the zirconium-carbon phase diagram in Figure 16. The ZrC + C eutectic temperature was found to be 2890° ± 50°C. The value of 2890° ± 50°C compares favorably with values of 2850° ± 50°C and 2920° ± 50°C reported by Sara et al[1], Storms[2], and Portnoy[3] et al, respectively.

The concentration independent diffusion coefficient of carbon in ZrC, D_C^{ZrC}, was calculated from the growth data and the zirconium-carbon phase diagram shown in Figure 16. The diffusion carbon concentration profile is shown in Figure 17.

The equations used to calculate the value of D_C^{ZrC} were

$$\frac{C_s - C_{II,\,I}}{C_{II,\,I} - C_o} = \sqrt{\pi}\ \gamma\ \exp^{\gamma^2}\ \mathrm{erf}\ (\gamma) \qquad (4)$$

(1) R. V. Sara, C. E. Lowell, and R. T. Dolloff, "Research Study to Determine the Phase Equilibrium Relations of Selected Metal Carbides at High Temperatures," WADD-TR-60-143, February, 1963, p. 16-17.
(2) E. K. Storms, Los Alamos Scientific Laboratory, LAMS-2674, March 15, 1962.
(3) K. I. Portnoy, Yu V. Levinsky, and V. I. Fadyeyeva, Izvest. Akad. Nauk SSR, Otdel, Tekh. Nauk, met. i Toplivo 2, p. 147 (1961).

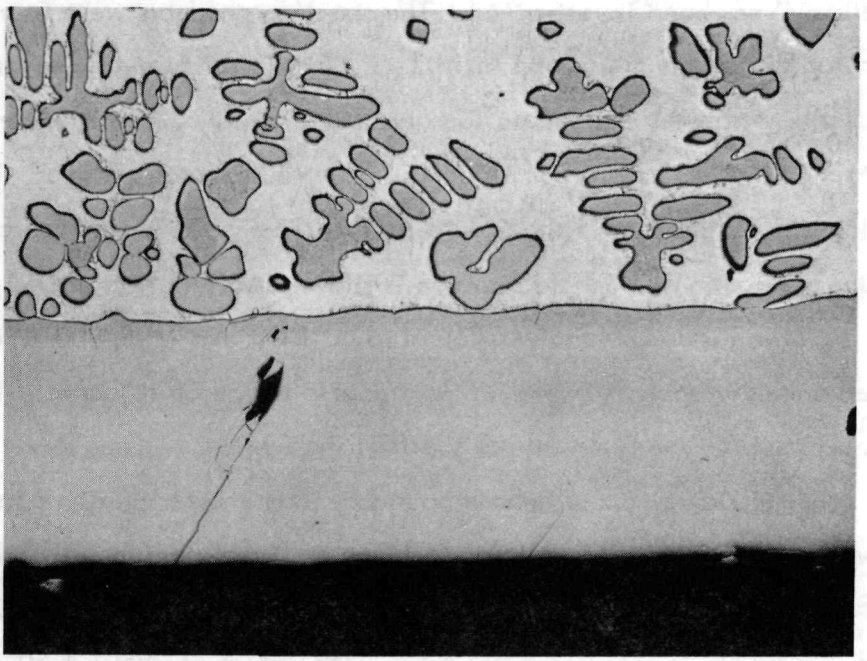

Figure 13 - Metallographic Section of Product of Zirconium-Carbon Reaction for 16 Minutes at 2750°C (100X)

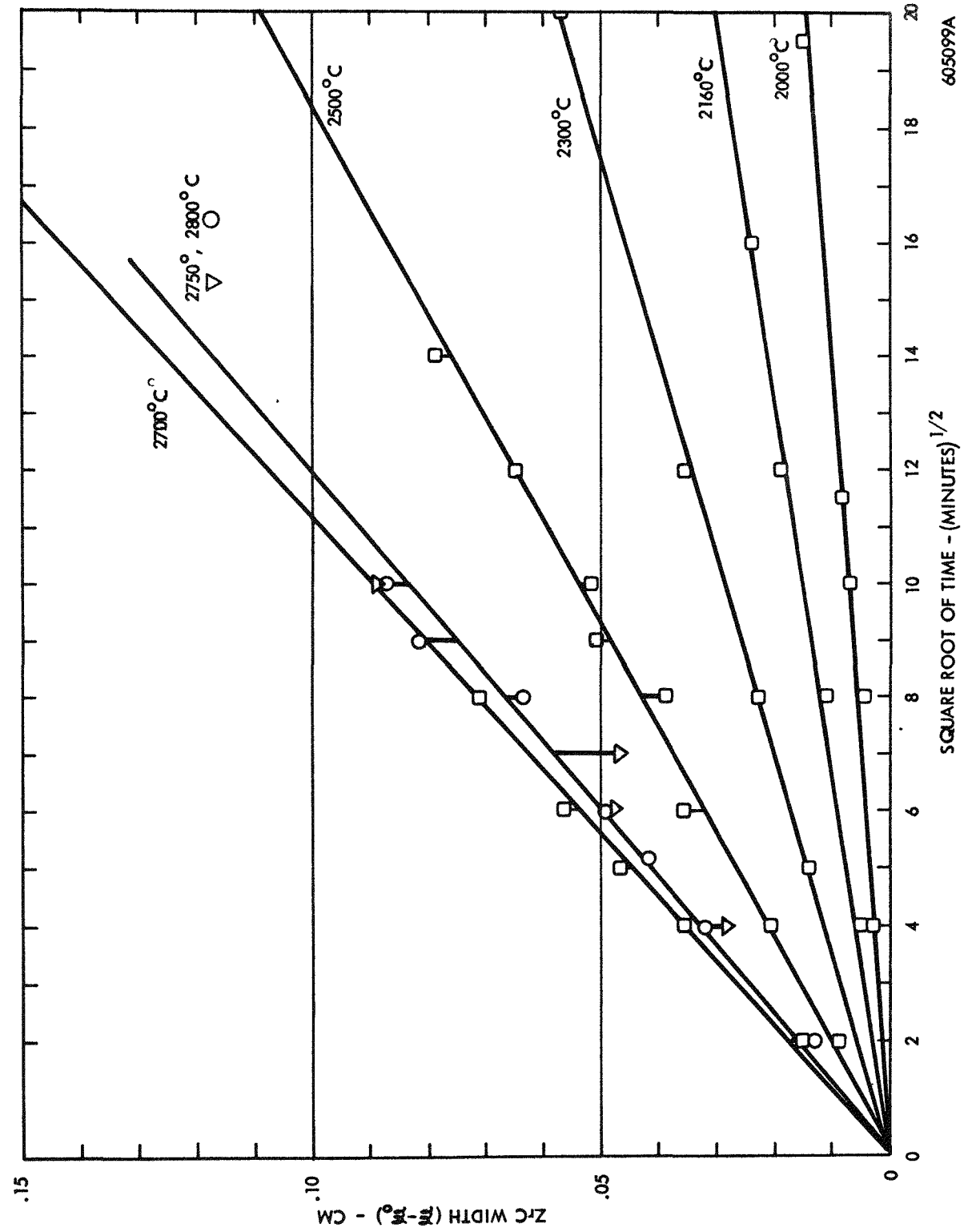

Figure 14 - Width of ZrC as a Function of the Square Root of Carburization Time

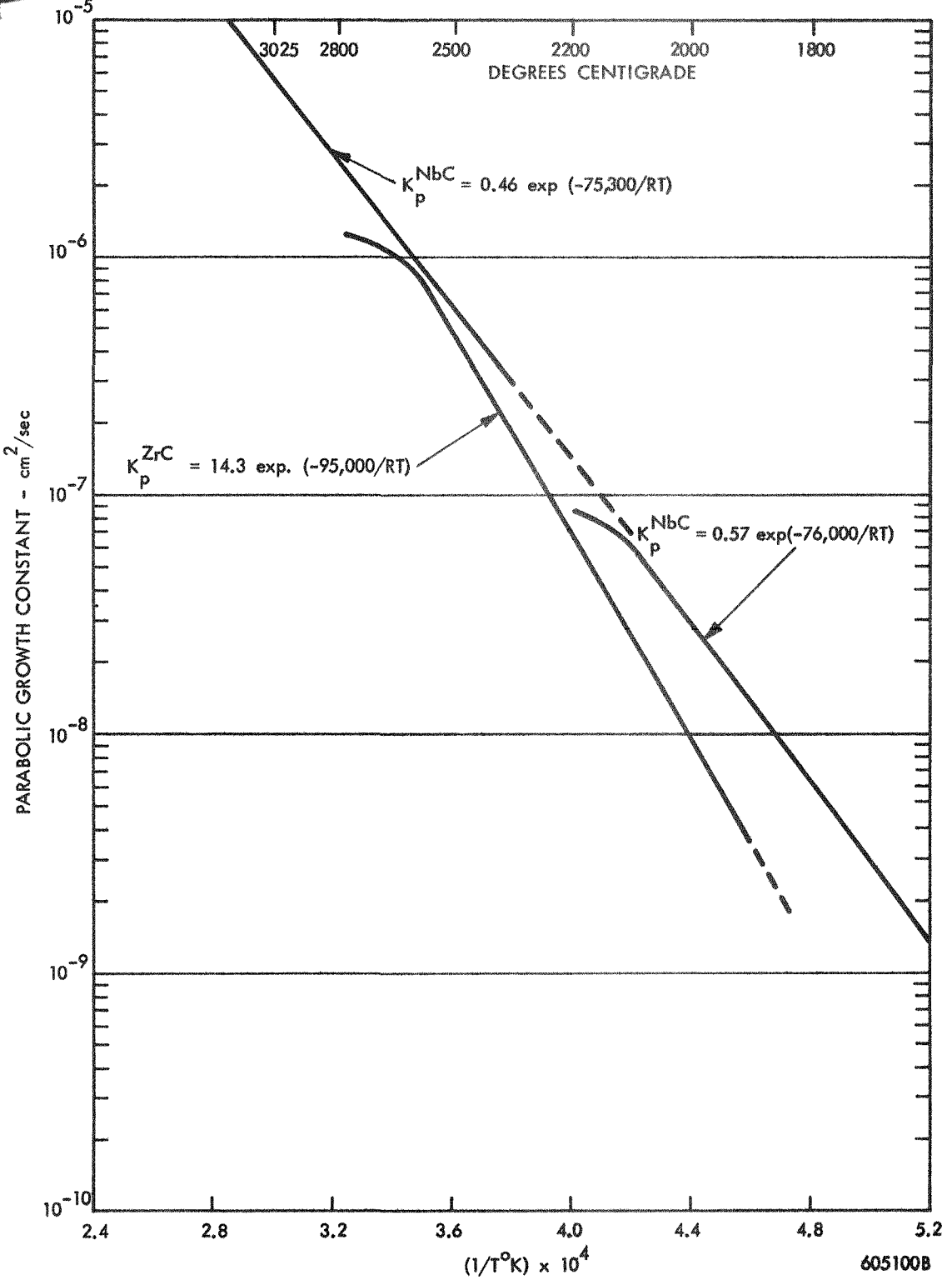

Figure 15 - Parabolic Growth Constant for ZrC and NbC as a Function of Inverse Temperature

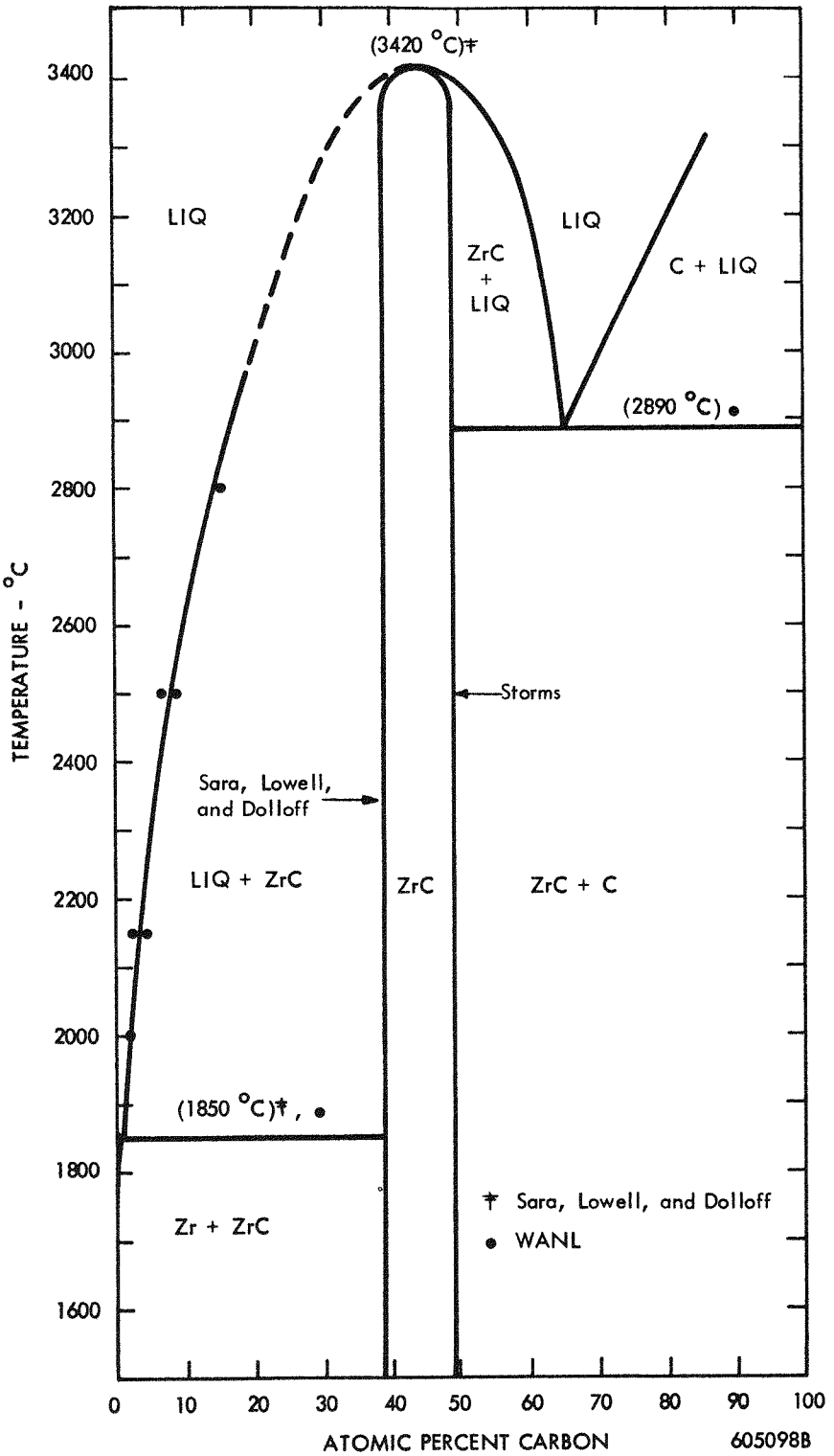

Figure 16 - Zirconium-Carbon Phase Diagram

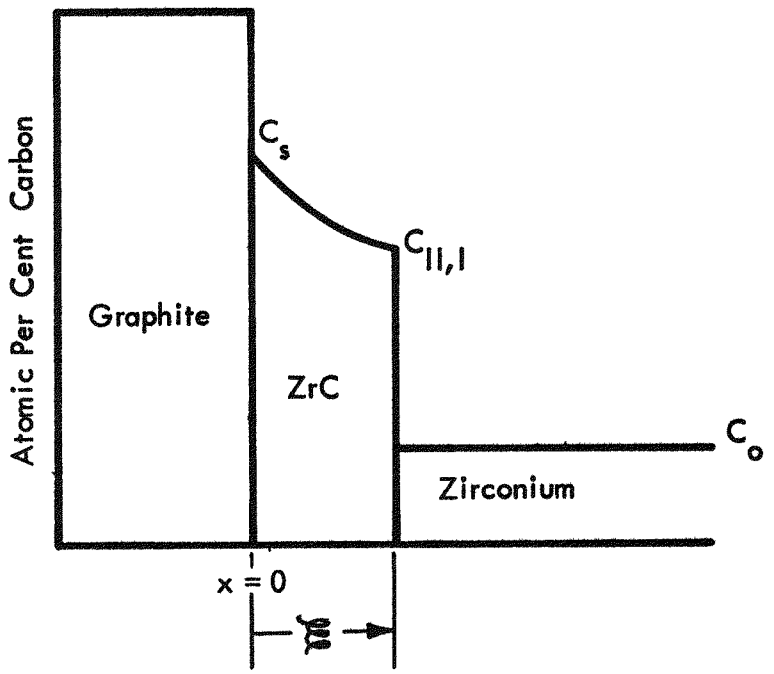

$$(1) \quad \frac{C_s - C_{II,I}}{C_{II,I} - C_o} = \sqrt{\pi}\,\gamma \exp \gamma^2 \operatorname{erf}(\gamma)$$

$$(2) \quad \gamma = \frac{x}{\sqrt{4Dt}}$$

Figure 17 - Carbon Profile for Diffusion in ZrC

and

$$D_C^{ZrC} = \Xi^2/4\gamma^2 t = K_p/4\gamma^2 \quad \text{(4 ref.)} \tag{5}$$

where

C_s = carbon concentration in ZrC at ZrC-C interface

$C_{II,I}$ = carbon concentration in ZrC at ZrC-liq interface

C_o = carbon concentration in the liquid

$\gamma = \Xi/\sqrt{4Dt}$

Ξ = is the width of the ZrC at a time t

K_p = parabolic rate constant.

The values of C_s and $C_{II,I}$ for calculating D_C^{ZrC} were taken from the data of Sara, Lowell, and Dolloff. The values of C_o at each temperature were determined in this study. An Arrhenius plot of the $D_C^{ZrC^o}$ is shown in Figure 18. The diffusion coefficient was found to be 34 exp (-96, 500/RT) cm^2/sec.

Niobium-Carbon System

The kinetics of the niobium-carbon reaction at temperatures between 2500° and 3200°C have been studied. This extends the range of the previously reported work to temperatures above the Nb melting point. Experimental runs to determine the Nb/(Nb + Nb_2C) and Nb/(Nb + NbC) phase boundaries to 3400°C have been completed.

Parabolic growth behavior of NbC was observed in the niobium-carbon reaction at temperatures between 2500° and 3200°C. The growth rate of the Nb_2C was too low to determine any growth behavior. The thickness of the NbC as a function of time is proportional to the square root of time. The activation energy for the NbC parabolic

(4) W. Jost, Diffusion in Solids, Liquids, Gases, Academic Press Inc., N. Y. 1960, p. 69, 70.

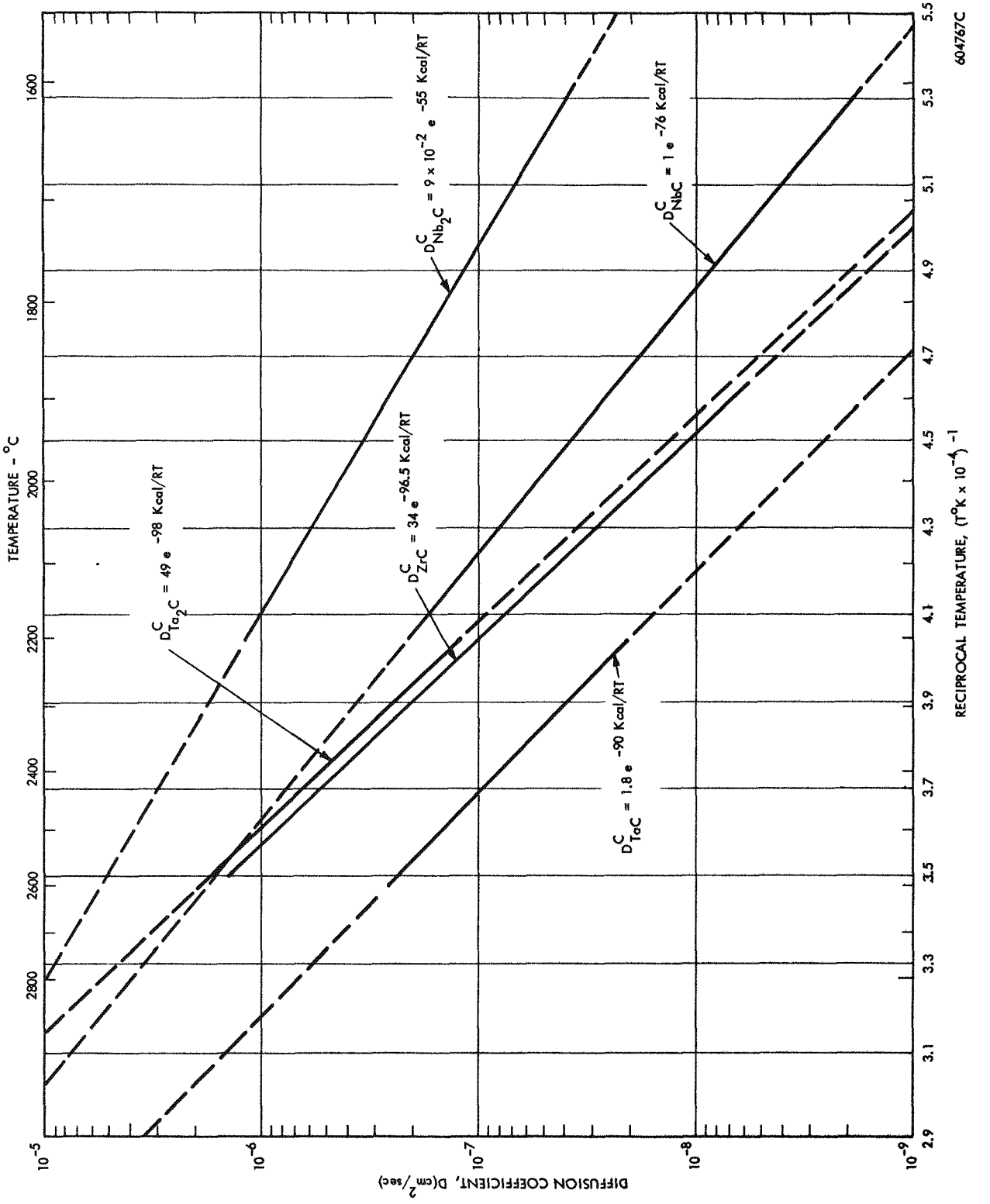

Figure 18 - Diffusion Coefficients in Carbides as a Function of Reciprocal Temperature

rate constant was determined from Figure 15. The parabolic rate constant for NbC was measured to be 0.46 exp (75,300/RT) cm^2/sec. The activation energy of 75,300 cal/mole agrees well with the value of 76,000 cal/mole reported by Brizes, Cadoff, and Tobin[4] for carbon diffusion in NbC at temperatures below 2300°C.

Preliminary results indicate that the Nb + NbC $\rightleftharpoons$ Nb_2C peritectic temperature is 3150° ± 50°C.

Tantalum-Carbon System

Preliminary results on the measurement of carbon diffusion in TaC and Ta_2C are shown in Figure 18. It should be noted that the carbon diffusion coefficient in TaC is approximately an order of magnitude lower than that in NbC. Coatings of TaC are being considered for development as a protective coating for graphite at higher temperatures than currently used for NbC coated graphite.

(4) W. Brizes, L. Cadoff, and J. M. Tobin, "Diffusion in the Niobium Carbon System," WANL-TNR-185, December, 1964.

III. ANALYSIS OF HYDROGEN CORROSION BEHAVIOR OF NERVA FUEL ELEMENTS (M. Blinn, G. R. Kilp, and A. Boltax)

Figure 19 presents a summary of hydrogen corrosion data obtained in the electrical test facility on NRX-A2, A3, and A4 fuel elements produced at the Westinghouse Astrofuel Facility (WAFF) and at the Y-12 plant at Oak Ridge, The overlap of the data for the various test conditions represents element to element variability and test temperature variability and uncertainty. The corrosion test data has been analyzed in terms of three principal mechanisms of carbon weight loss. The corrosion mechanisms include: corrosion at cracks in the NbC coating; corrosion in defects in the NbC coating (other than cracks); and carbon diffusion through the NbC coating. The results of this analysis will be reviewed briefly.

Figure 20 provides the basic corrosion rate data used in the analysis of corrosion behavior of NERVA fuel elements. The data given for fueled graphite, unfueled graphite, and pyrolytic carbon were obtained from hydrogen corrosion experiments at 40 atmospheres. The corrosion rate data shown for NbC and TaC coated graphite were obtained from calculations based on the measured diffusion rates of carbon in NbC and TaC, respectively.

Fueled graphite coated with NbC shows evidence of hydrogen corrosion between 1300° and 1800°C, particularly in the vicinity of cracks in the NbC coating. This form of corrosion attack, called mid-range corrosion, appears locally as undercutting of the graphite beneath cracks in the NbC coating. The cracks of the coating are present as a direct consequence of the difference of the coefficient of the thermal expansion between the NbC coating and the fueled graphite substrate. Cracks are closed in regions of the fuel element operated at temperatures above the temperature used in the vapor deposition process, i.e. 1900°C.

The equation used to describe carbon weight loss below 1900°C by the mid-range corrosion mechanism is given below:

$$\Delta W = K_{\ell} \Delta T \Delta \alpha \exp(-\Delta H/RT) \qquad (6)$$

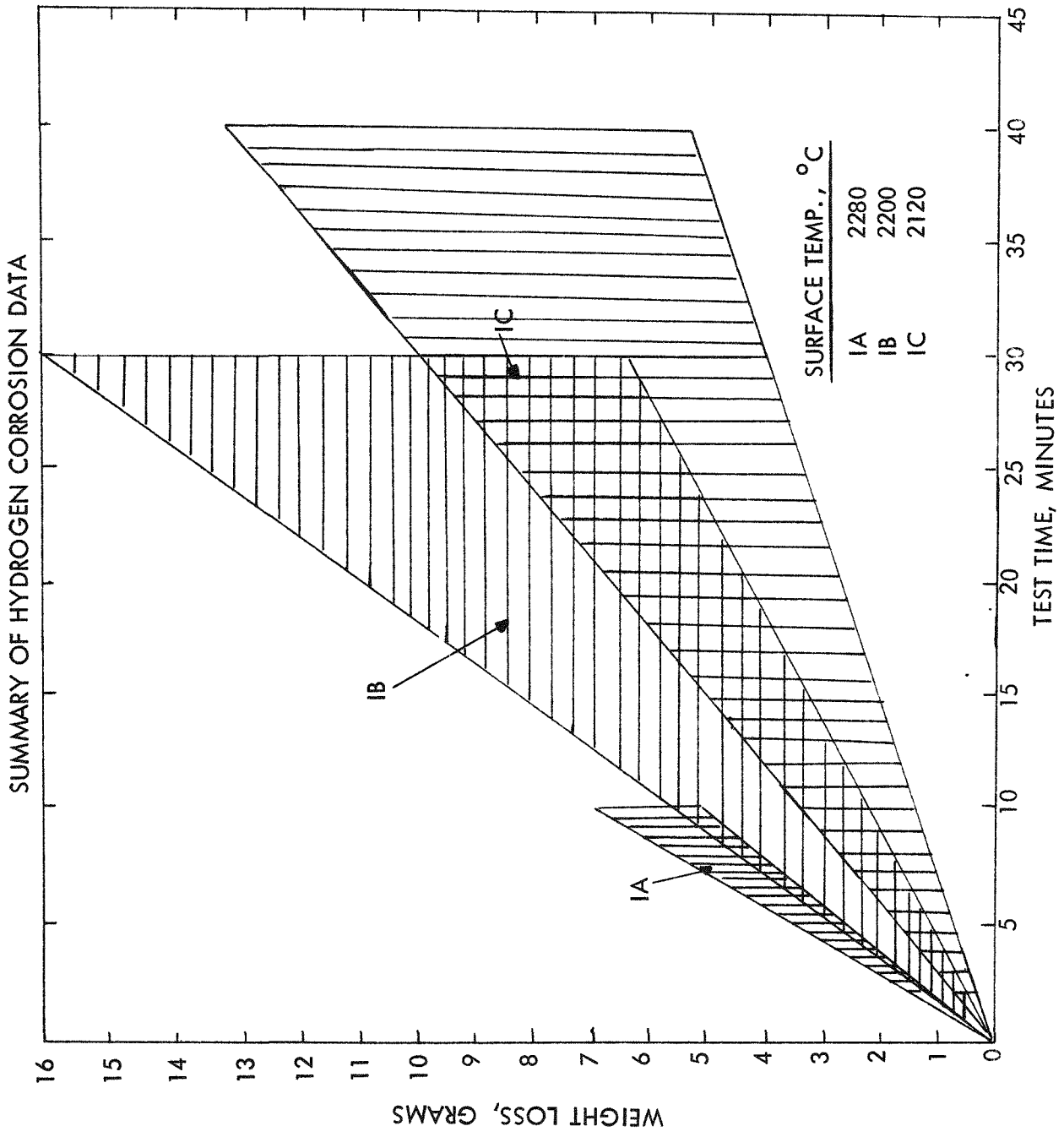

Figure 19 - Summary of Hydrogen Corrosion Data

CORROSION RATE DATA

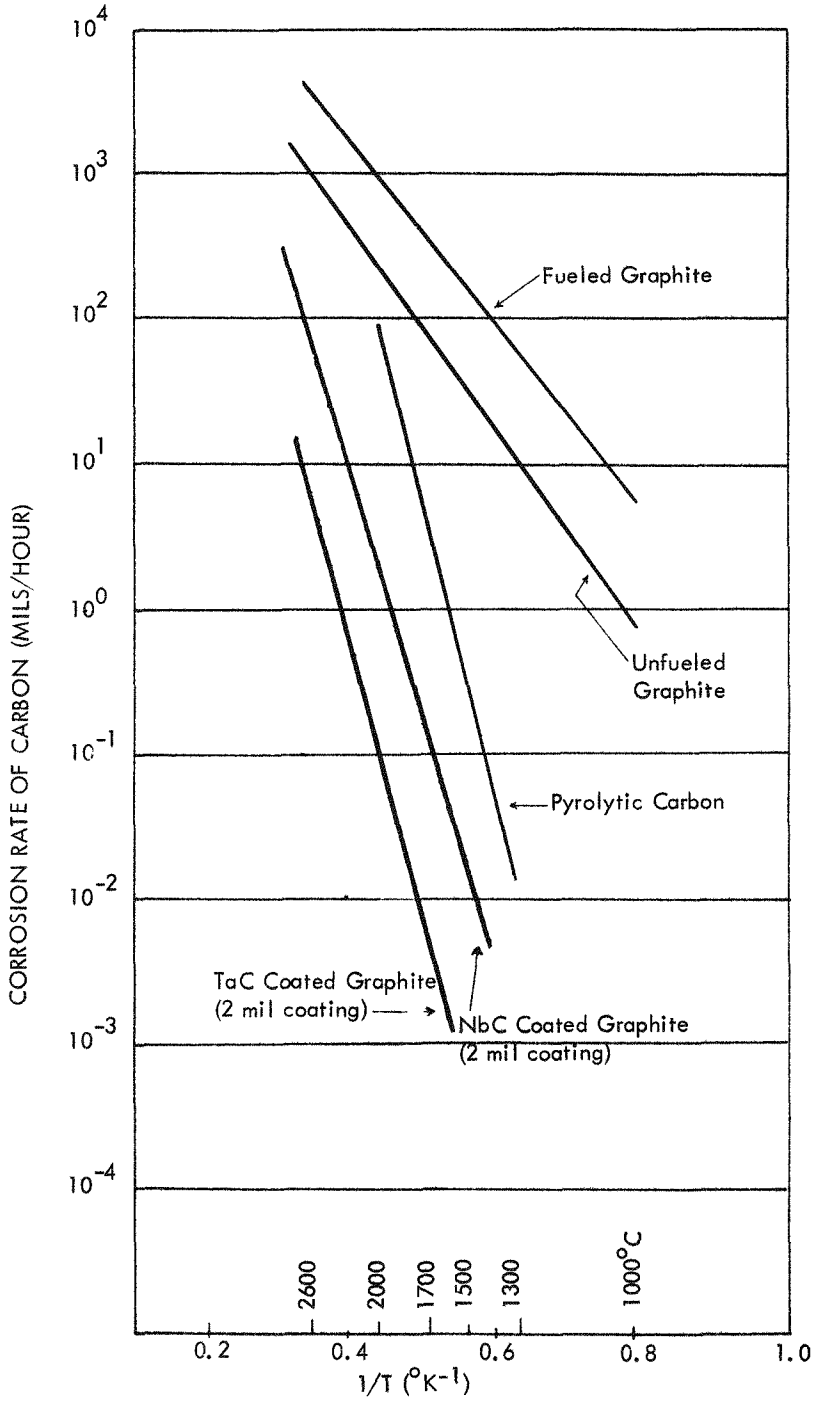

Figure 20 - Corrosion Rate Data

where ΔW is the weight loss in grams per minute per unit length, K_1 a constant, ΔT the difference in the coating temperature, 1900°C, and the temperature of interest T in °K, $\Delta\alpha$ is the differential contraction of the NbC and fueled graphite at the temperature of interest, ΔH is the activation energy for corrosion of fueled graphite (30,000/mole), and R is the gas constant. The total (per element) weight loss due to mid-range corrosion is obtained by integrating the weight loss over the length of the fuel element at temperatures from 800° to 1900°C. Preliminary integrated weight loss values of 0.2 to 0.25 grams/minute have been determined.

At temperatures above 1900°C NbC coating temperature, the mechanism of hydrogen corrosion attack of coated graphite involves decarburization of the NbC coating and subsequent diffusion of carbon through the coating, as well as local corrosion at defects in the NbC coating. The decarburization mechanism is controlled by the rate of carbon diffusion through NbC and can be described by the following equations. The flux J (grams/second) of carbon diffusing through coating is given by:

$$J = -DA\,\delta c/\delta x \tag{7}$$

where D is the diffusion coefficient for carbon in NbC in cm^2/sec, A is the area, and $\delta c/\delta x$ is the carbon concentration gradient within the NbC coating, expressed in $grams/cm^3$. D is a function of temperature and has been determined recently by Brizes and Cadoff[4] to be:

$$D = 1.0 \exp(-76,000/RT) \tag{8}$$

The concentration gradient $\delta c/\delta x$ depends upon coating thickness and C/Nb stoichiometry at the graphite coating interface and at the coating hydrogen interface. Generally, the C/Nb ratio is approximately 1 at the graphite-coating interface and 0.75 at the hydrogen-coating surface at hot end of fuel elements.

The equation describing the decarburization weight loss at a given temperature is as follows:

$$\Delta W = K_2 \exp(-76,000/RT)/d \tag{9}$$

where ΔW is the weight loss in grams per minute per unit length, K_2 a constant depending upon carbon concentration gradient, and d the NbC coating thickness. The total (per element) weight loss due to decarburization corrosion is obtained by intergrating the weight loss over the length of the element of at temperatures above 1900°C. Preliminary integrated weight loss values for the corrosion tests, the 1A, 1B, and 1C corrosion tests have been calculated and are given in Table 1.

The major conclusions resulting from this analysis are that mid-range corrosion accounts for a large fraction of the total fuel element weight loss and that corrosion through NbC coating defects increases with increasing corrosion test time. Therefore, improvement in the performance of the NbC coating at the center of the fuel element would result in significantly lower overall fuel element weight loss. Development programs are currently in progress to minimize the extent of mid-range corrosion.

Table 1 - Quantitative Analysis of Hydrogen Corrosion Results

Corrosion Test	Weight Loss Per Unit Time, gms/min.				
	Observed Rates		Calculated Rates		
	Max.	Min.	Mid-range Corrosion*	Decarburization Corrosion	Max. Corrosion Through Defects*
1A	0.70	0.50	0.20-0.25	0.35	< 0.1
1B	0.53	0.22	0.20-0.25	0.13	< 0.15
1C	0.33	0.13	0.20-0.25	0.05	< 0.05

* Detailed examination of the corrosion data indicates that corrosion through defects (both cracks and other defects) increases with increasing test time and number of thermal cycles. This effect becomes important for 2 or more cycle tests for times of 30 minutes and longer.